References

ACTON, A. F. & BEVIS, M. (1971). *Acta Cryst.* A**27**, 175–179.

BISHOP, G. & CHALMERS, B. (1968). *Scripta Met.* **2**, 133–139.

BOLLMANN, W. (1970). *Crystal Defects and Crystalline Interfaces*. Berlin: Springer.

BOLLMANN, W., MICHAUT, B. & SAINFORT, G. (1972). *Phys. Stat. Sol.* **13**, 637–649.

BRANDON, D. G. (1966). *Acta Met.* **14**, 1479–1484.

BRANDON, D. G., RALPH, B., RANGANATHAN, S. & WALD, M. S. (1964). *Acta Met.* **12**, 813–821.

CHAUDHARI, P. & MATTHEWS, J. W. (1970). *Appl. Phys. Lett.* **17**, 115–117.

CHAUDHARI, P. & MATTHEWS, J. W. (1971). *J. Appl. Phys.* **42**, 3063–3066.

DICKSON, L. E. (1957). *Introduction to the Theory of Numbers*. New York: Dover.

FRIEDEL, G. (1964). *Leçons de Cristallographie*. Paris: Blanchard. (Reprint of 1926 edition.)

FORTES, M. A. (1972). *Phys. Stat. Sol.* **54**, 311–319.

International Tables for X-ray Crystallography (1969). Vol. I. Birmingham: Kynoch Press. The earlier editions do not contain the contribution on reduced cells by A. D. MIGHELL, A. SANTORO and J. D. H. DONNAY.

ISHIDA, Y. & MCLEAN, M. (1973). *Phil. Mag.* **27**, 1125–1134.

PUMPHREY, P. H. & BOWKETT, K. M. (1971). *Scripta Met.* **5**, 365–369.

RANGANATHAN, S. (1966). *Acta Cryst.* **21**, 197–199.

SANTORO, A. & MIGHELL, A. D. (1973). *Acta Cryst.* A**29**, 169–175.

SCHOBER, T. & BALLUFFI, R. W. (1970). *Phil. Mag.* **21**, 109–123.

SCHOBER, T. & BALLUFFI, R. W. (1971). *Phil. Mag.* **24**, 165–180.

SCHOBER, T. & BALLUFFI, R. W. (1971). *Phys. Stat. Sol.* (*b*) **44**, 115–126.

TU, K. N. (1971). *Scripta Met.* **5**, 537–541.

WARRINGTON, D. H. & BOLLMANN, W. (1972). *Phil. Mag.* **25**, 1195–1199.

WARRINGTON, D. H. & BUFALINI, P. (1971). *Scripta Met.* **5**, 771–776.

WOIRGARD, J. & DE FOUQUET, J. (1972). *Scripta Met.* **6**, 1165–1174.

Acta Cryst. (1974). A**30**, 207

Instrumental Widths and Intensities in Neutron Crystal Diffractometry

BY B. GRABCEV

Institute for Atomic Physics, Bucharest, P.O. Box 35, *Romania*

(*Received* 13 *March* 1973; *accepted* 7 *August* 1973)

The amplitude and the shape of the quasielastic resolution function of a neutron two-axis spectrometer are calculated in the Gaussian approximation. Special attention is given to the explicitness of the formulae as well as to their absolute correctness, avoiding any unknown proportionality factors. The results are applied to the analysis of the elastic scattering of neutrons in crystals.

1. Introduction

In an experiment to analyse the angular distribution of scattered neutrons, carried out with a crystal diffractometer (two-axis spectrometer), the finite collimations, the monochromator mosaic structure and the beam-path configuration influence both the counting rate and the experimental line width. This influence should be quantitatively described by an instrumental function, the so-called resolution function.

The knowledge of the resolution function makes possible the choice of advantageous experimental conditions as well as the correct interpretation of experimental data. That is why great attention has been paid to the problem of determining the dependence of the diffractometer resolution function on all experimental factors.

The early papers in which resolution effects were considered deal with elastic-scattering experiments, their principal aim being the calculation of Bragg peak width and relative intensities for some usual experimental methods (Caglioti, Paoletti & Ricci, 1958, 1960; Caglioti & Ricci, 1962; Sailor, Foote, Landon & Wood, 1956; Willis, 1960).

In a more general treatment, Cooper & Nathans (1968*a*) have shown, also for elastic experiments, that the counting rate is given by the convolution, in the space of wave-vector transfers $\mathbf{Q}$ ($\mathbf{Q}=\mathbf{k}_i-\mathbf{k}_f$), of the scattering cross section with the resolution function

$$I(\mathbf{Q}_0)=\int \sigma(\mathbf{Q})R(\mathbf{Q})\mathrm{d}\mathbf{Q}\,.$$

$\mathbf{Q}_0$ is the nominal setting of the instrument as defined by the most probable wave vectors $\mathbf{k}_I$ and $\mathbf{k}_F$. In the Gaussian approximation, assuming that both the transmission functions of collimators and the reflectivity of the monochromator crystal are Gaussian-like functions, the elastic resolution function of the diffractometer can be written

$$R(\mathbf{Q}_0+\mathbf{X})=R_0\exp\{-\tfrac{1}{2}\sum_{i,j=1}^{3}M_{ij}X_iX_j\} \qquad (1)$$

where X_1, X_2, X_3 are the Cartesian components of $\mathbf{X}=\mathbf{Q}-\mathbf{Q}_0$. X_1 is chosen parallel to $-\mathbf{Q}_0$ and X_3 is vertical (perpendicular to the scattering plane). R_0 and M_{ij} depend on $\mathbf{Q}_0$ as well as on instrumental parameters.

The case of an inelastic experiment performed on a two-axis spectrometer has recently been considered by Tucciarone, Lau, Corliss, Delapalme & Hastings (1971).

In the treatment presented below the Cooper–Nathans formulation is extended to derive the quasielastic resolution function of a neutron two-axis spectrometer, the quasielastic scattering process being considered as the most general case for which the two-axis analysis represents a really efficient experimental method.

As for many physical systems (*e.g.* polycrystals, liquids, paramagnetics) the scattering cross section is a function of Q rather than of $\mathbf{Q}$, this case is considered separately in order to obtain the most simple, straightforward relations between resolution function and instrumental parameters.

Special attention is attached to the explicitness of the formulae as well as to their absolute correctness, avoiding any unknown proportionality factors.

The results are used to reconsider the elastic scattering of neutrons in perfect as well as in mosaic imperfect crystals, by calculating the width and absolute value of the integrated intensity of a Bragg peak as obtained in a general linear scan.

For the sake of brevity mathematical derivations and some applications are given in an Appendix.

2. Quasielastic resolution function of a two-axis neutron spectrometer

The first step in the derivation of the resolution function is to define the counting rate as an average of the scattering cross section over the space and energy distributions of neutrons in the incoming and scattered beams. For a given setting the counting rate may be written as

$$I(\mathbf{k}_I,\mathbf{k}_F)=N\int \Phi(\mathbf{k}_i)T_M(\mathbf{k}_i,\mathbf{k}_I)\frac{\mathrm{d}\sigma}{\mathrm{d}\mathbf{k}_f} \times T_A(\mathbf{k}_f,\mathbf{k}_F)\varepsilon(k_f)\mathrm{d}\mathbf{k}_i\mathrm{d}\mathbf{k}_f\,. \quad (2)$$

N is the number of atoms (or unit cells) in the sample. $\Phi(\mathbf{k})$ is the $\mathbf{k}$ density of the neutron flux [$\Phi(\mathbf{k})=\Phi_0 k\exp(-k^2/k_T^2)/2\pi k_T^4$, where Φ_0 is the total thermal flux and $k_T=(2mk_BT)^{1/2}/\hbar$]. $T_M(\mathbf{k}_i,\mathbf{k}_I)$ is the transmission function of the monochromator system for $\mathbf{k}_i$ neutrons when the $\mathbf{k}_I$ neutrons are preferentially transmitted. $\mathrm{d}\sigma/\mathrm{d}\mathbf{k}_f$ is the scattering cross section of the sample per atom (or unit cell) and volume unit in $\mathbf{k}_f$ space. $T_A(\mathbf{k}_f,\mathbf{k}_F)$ has the same meaning as $T_M(\mathbf{k}_i,\mathbf{k}_I)$ but for the analysing system. $\varepsilon(k_f)$ is the detector counting efficiency for k_f neutrons.

In the next stage, the variables defining the cross section are introduced in equation (2) to replace an equal number of the six variables $(\mathbf{k}_i,\mathbf{k}_f)$. The integration over the remaining variables yields the resolution function. Generally, when the inelastic processes are analysed on a two-axis spectrometer, this integration may not be performed. However, for quasielastic scattering cross sections, under special experimental conditions which make sure that in the scattered beam the neutron energy distribution represents a narrow band around E_I (the most probable incident energy) so that the slowly varying functions of k_f can be replaced by their values in k_I, the integration becomes possible producing an explicit analytical expression for the resolution function. This requirement may be achieved by a suitable choice of the instrumental parameters. For instance, if the scattering cross section is Lorentzian with half width ΔE:

$$\frac{\mathrm{d}^2\sigma}{\mathrm{d}\Omega\mathrm{d}E_f}\sim\frac{(\Delta E)^2}{(\Delta E)^2+(E_i-E_f)^2}\,,$$

the half width of the neutron energy distribution in the incoming beam [with the notation of Cooper & Nathans (1967)]

$$\Delta E_I=\frac{E_I}{2}\,|\mathrm{ctg}\,\theta_M|\left(2\ln 2\,\frac{\eta_M^2\alpha_0^2+\eta_M^2\alpha_1^2+\alpha_0^2\alpha_1^2}{\alpha_0^2+4\eta_M^2+\alpha_1^2}\right)^{1/2} \quad (3)$$

must be fixed at a value which allows the convolution of the cross section with the incident neutron intensity

$$J(E_i)=J(E_I)\exp\left[-\ln 2(E_i-E_I)^2/(\Delta E_I)^2\right]$$

to be sufficiently narrow. The half width of the convolution of a Lorentzian with a Gaussian has been calculated by Teutsch (1971); when $\Delta E_I\lesssim\Delta E$, *e.g.*, it is smaller than $\sim 1{\cdot}6\Delta E$. If necessary, more severe restrictions may be imposed on the ratio $\Delta E_I/\Delta E$ through equation (3).

The derivation of the $(\mathbf{Q},\omega)$ and the (Q,ω) resolution functions is briefly explained in the Appendix. A more detailed mathematical treatment is given in a preprint (Grabcev, 1973*a*).

The $(\mathbf{Q},\omega)$ *resolution function*

As shown in the Appendix, for a quasielastic cross section, when the scattering angle is much larger than

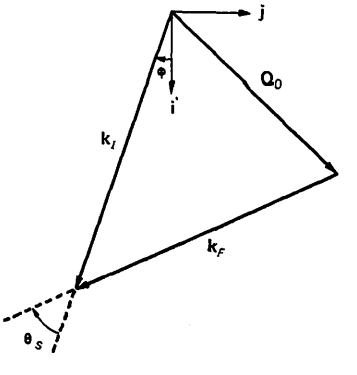

Fig. 1. Vector diagram in reciprocal space for the most probable scattering process.

the collimation angles (*i.e.* the small-angle scattering case is excluded) and the instrumental parameters are chosen in the sense of the discussion at the begining of § 2, the counting rate may be written as

$$I(\mathbf{k}_I,\mathbf{k}_F)=I(\mathbf{Q}_0)=\Phi(\mathbf{k}_I)\varepsilon(k_I) \times\int S(\mathbf{Q}_0,\mathbf{X},X_4)R(\mathbf{Q}_0,\mathbf{X},X_4)\mathrm{d}\mathbf{X}\mathrm{d}X_4 \quad (4)$$

where $X_4=\omega=(\hbar/2m)\,(k_i^2-k_f^2)$, $S=N\hbar\,\mathrm{d}^2\sigma/\mathrm{d}\Omega\mathrm{d}E_f$ while $R(\mathbf{Q}_0,\mathbf{X},X_4)$ is the resolution function.

In this definition, the resolution function is a dimensionless quantity expressing the relative sensitivity of the instrument for a scattering process characterized by $\hbar(\mathbf{Q}_0+\mathbf{X})$ and $\hbar X_4$ momentum and energy transfer, when the diffractometer nominal setting corresponds to $\hbar\mathbf{Q}_0$ momentum transfer and the most probable process is an elastic one.

In the Gaussian approximation the resolution function is given by

$$R(\mathbf{Q}_0,\mathbf{X},X_4)=R_0(\mathbf{Q}_0)\exp\left[-\tfrac{1}{2}\sum_{i,j=1}^{4}M_{ij}(\mathbf{Q}_0)X_iX_j\right], \quad (5)$$

where X_1, X_2, X_3 have the same meaning as in equation (1), the only difference being the arbitrary orientation of the **i** axis relative to the scattering vector (Fig. 1); for a certain physical situation it may be particularized in a suitable mode.

The (Q,ω) resolution function

When the scattering cross section is expressed in terms of the magnitude of the momentum transfer it is convenient to define a corresponding resolution function depending on this variable too. In this case the counting rate takes the following form:

$$I(Q_0)=\Phi(k_I)\varepsilon(k_I) \times\int S(Q_0,X_1,X_4)\mathscr{R}(Q_0,X_1,X_4)\mathrm{d}X_1\mathrm{d}X_4 \quad (6)$$

where $X_1=Q-Q_0$ while $\mathscr{R}(Q_0,X_1,X_4)$ is the (Q,ω) resolution function, given by:

$$\mathscr{R}(Q_0,X_1,X_4)=\mathscr{R}_0(Q_0) \times\exp\left\{-\tfrac{1}{2}(\mathscr{M}_{11}X_1^2+2\mathscr{M}_{14}X_1X_4+\mathscr{M}_{44}X_4^2)\right\}. \quad (7)$$

In order to define the (Q,ω) resolution function as a dimensionless quantity as well, the k density of the neutron flux, $\Phi(k)=4\pi k^2\Phi(\mathbf{k})$, has been introduced in equation (6).

Between $R(\mathbf{Q},\omega)$ and $\mathscr{R}(Q,\omega)$ the following relations may be found:

$$\mathscr{R}_0=\frac{R_0}{2k_I^2(M_{22}M_{33})^{1/2}} \quad (8a)$$

$$\mathscr{M}_{ij}=M_{ij}-\frac{M_{i2}M_{2j}}{M_{22}}\,. \quad (8b)$$

Even if the two-axis spectrometer provides no energy resolution, there exists an explicit dependence of its resolution function on energy transfer, which must be taken into account in quasielastic experiments (*e.g.* critical scattering with $\tau\neq 0$, quasielastic scattering in liquids) to correct the angular distribution data for inelastic effects.

The presence of $\delta(\omega)$ in elastic-scattering cross sections cancels the energy-dependent part of the resolution function, the counting rate being given in this case by

$$I(\mathbf{Q}_0)=\Phi(\mathbf{k}_I)\varepsilon(k_I)\int S(\mathbf{Q}_0,\mathbf{X})R(\mathbf{Q}_0,\mathbf{X})\mathrm{d}\mathbf{X} \quad (9)$$

or

$$I(Q_0)=\Phi(k_I)\varepsilon(k_I)\int S(Q_0,X_1)\mathscr{R}(Q_0,X_1)\mathrm{d}X_1 \quad (10)$$

where:

$$R(\mathbf{Q}_0,\mathbf{X})=R_0(\mathbf{Q}_0)\exp\left\{-\tfrac{1}{2}\sum_{i,j=1}^{3}M_{ij}X_iX_j\right\} \quad (11)$$

and

$$\mathscr{R}(Q_0,X_1)=\mathscr{R}_0(Q_0)\exp\left\{-\tfrac{1}{2}\mathscr{M}_{11}X_1^2\right\} \quad (12)$$

are the elastic resolution functions while $S=N\mathrm{d}\sigma/\mathrm{d}\Omega$.

Equations (4) and (6) make possible the calculation of widths and intensities in any experimental situation as well as attempts to find how the instrumental parameters (incident neutron energy, collimation, monochromator crystal) should be changed in order to give more advantageous experimental conditions.

The explicit analytical formulae for the $(\mathbf{Q},\omega)$ and the (Q,ω) resolution functions are given in the Appendix. The unconventional nomenclature used there [equations (33) and (37)] is more convenient for the explicitness of the formulae. Moreover, a unified notation for the horizontal collimation angles and mosaic spread of the monochromator system [the m_i coefficients from equation (33)] is imposed by the remarkable equivalence of these elements in the expression for the resolution function. $a_1=1/2\alpha_2^2$ is a remnant of a similar notation used for the analysing system in a paper devoted to the resolution function of a triple-axis spectrometer (Grabcev, 1973*b*). Although the resolution function of the diffractometer may be obtained from that derived for a triple-axis spectrometer by putting $k_F=\mathrm{tg}\,\theta_A=k_I$, $P_A=1$, $\alpha_3=\beta_3=\eta_A=\infty$, it has been considered here independently both to avoid the necessity of knowing details concerning triple-axis spectroscopy and to outline the salient features of the two-axis analysis.

3. Application to the analysis of elastic scattering of neutrons in crystals

The equation of the diffraction pattern of a perfect single crystal is obtained by introducing in equation (9) the elastic coherent scattering cross section (Cassels, 1951):

$$\frac{\mathrm{d}\sigma}{\mathrm{d}\Omega}=\frac{(2\pi)^3}{V_c}\,|F(\mathbf{Q})|^2\sum_{\tau}\delta(\mathbf{Q}+2\pi\boldsymbol{\tau})$$

where V_c is the volume of the unit cell, $F(\mathbf{Q})$ is the structure factor including the Debye–Waller factor and $\boldsymbol{\tau}$ is any vector in the reciprocal lattice of the sample. There results:

$$I(\mathbf{Q}_0)=N\frac{(2\pi)^3}{V_c}\Phi(\mathbf{k}_I)\varepsilon(k_I)\sum_{\boldsymbol{\tau}}|F(-2\pi\boldsymbol{\tau})|^2R_0(-2\pi\boldsymbol{\tau})\times\exp\{-\tfrac{1}{2}\sum_{i,j=1}^{3}M_{ij}(Q_{0i}+2\pi\tau_i)(Q_{0j}+2\pi\tau_j\}, \quad (13)$$

i.e. a set of peaks whose widths and intensities are essentially determined by the resolution function.

For a certain $\boldsymbol{\tau}$, putting

$$\mathbf{q}=\mathbf{Q}_0+2\pi\boldsymbol{\tau},$$

equation (13) indicates that the locus of points in $\mathbf{Q}$ space for which the counting rate is p times smaller than in the Bragg position ($\mathbf{Q}_0=-2\pi\boldsymbol{\tau}$) is an ellipsoid:

$$M_{11}q_1^2+2M_{12}q_1q_2+M_{22}q_2^2+M_{33}q_3^2=2\ln p. \quad (14)$$

Consequently, the shape of a Bragg peak is dependent on the direction of displacement in $\mathbf{Q}$ space during the scan. Equation (13) makes possible the calculation of width and intensity for any scan. However, only linear scans will be considered here, there being no evident advantage for a scan whose trajectory in $\mathbf{Q}$ space is a more or less complicated curve.

If $q_{\xi\zeta}$ (ξ and ζ are coordinates in $\mathbf{q}$ space given by:

$$\begin{aligned}q_1&=q_{\xi\zeta}\cos\xi\cos\zeta\\ q_2&=q_{\xi\zeta}\sin\xi\cos\zeta\\ q_3&=q_{\xi\zeta}\sin\zeta,\end{aligned} \quad (15)$$

the Bragg peak measured along a fixed, arbitrary direction, defined by the angles ξ and ζ) is described by:

$$I(\theta_B,q_{\xi\zeta})=I(\theta_B)\exp[-\tfrac{1}{2}M(\xi\zeta)q_{\xi\zeta}^2] \quad (16)$$

where:

$$M(\xi\zeta)=M_{11}\cos^2\xi\cos^2\zeta+2M_{12}\cos\xi\sin\xi\cos^2\zeta+M_{22}\sin^2\xi\cos^2\zeta+M_{33}\sin^2\zeta, \quad (17)$$

while $I(\theta_B)$ is the maximum intensity:

$$I(\theta_B)=N\frac{(2\pi)^3}{V_c}\Phi(\mathbf{k}_I)\varepsilon(k_I)|F(-2\pi\boldsymbol{\tau})|^2R_0(-2\pi\boldsymbol{\tau}). \quad (18)$$

Therefore, the Bragg peaks are Gaussians whose integrated intensities and half widths at half-maximum are given by:

$$I(\xi\zeta)=\int I(\theta_B,q_{\xi\zeta})\mathrm{d}q_{\xi\zeta}=I(\theta_B)\left[\frac{2\pi}{M(\xi\zeta)}\right]^{1/2} \quad (19)$$

and

$$L(\xi\zeta)=\left[\frac{2\ln 2}{M(\xi\zeta)}\right]^{1/2}. \quad (20)$$

The M_{ij} coefficients defining in equation (14) the equi-intensity ellipsoids are nothing other than the elements of the resolution matrix corresponding to $\mathbf{Q}_0=-2\pi\boldsymbol{\tau}$. That means that, at these particular points of $\mathbf{Q}$ space, $R(\mathbf{Q})$ may be directly determined experimentally from the widths and integrated intensities of Bragg peaks of a perfect crystal, measured in various scanning modes (Cooper & Nathans, 1968*b*).

By a proper choice of the reference frame the resolution ellipsoids can be directly visualized in the reciprocal lattice of the sample.

Equations (19) and (20) are used in the Appendix to derive the integrated intensities and half widths of Bragg peaks of a perfect crystal, corresponding to several conventional scans.

The coherent-scattering cross section of a mosaic crystal may be found by averaging the cross section of a perfect crystal with respect to the mosaic-block distribution (Cooper & Nathans, 1968*a*). From this (see the Appendix), there results the following expression for the counting rate:

$$I'(\mathbf{Q}_0)=I'(\theta_B)\exp[-\tfrac{1}{2}(M'_{11}q_1^2+2M'_{12}q_1q_2+M'_{22}q_2^2+M'_{33}q_3^2)] \quad (21)$$

where $I'(\theta_B)$ and M'_{ij} are dependent on the mosaic spread of the sample as well as on the diffractometer resolution function. Consequently, the formulae established for the widths and integrated intensities of a perfect crystal are valid in this case too, provided $I(\theta_B)$ and M_{ij} are replaced by $I'(\theta_B)$ and M'_{ij} respectively. The results obtained for some particular linear scans are listed in Table 2.

The (Q,ω) resolution function is used in the Appendix to derive the equation for the diffraction pattern of a polycrystal and the intensity of the incoherent background.

The expressions for half widths and integrated intensities collected in Table 2 and equations (86) are in agreement with those reported by Caglioti, Paoletti & Ricci (1958, 1960) and Caglioti & Ricci (1962) and (or) by Cooper (1968) and Cooper & Nathans (1968*b*). Moreover, here are given the absolute values of intensities as well as their dependence on vertical collimation and mosaic spreads.

APPENDIX

Derivation of the (Q, ω) resolution function

The notation is, generally, that of Cooper & Nathans (1967). γ_i and α_i are the horizontal divergence and collimation angles; δ_i and β_i are their corresponding vertical components. $i=0,1,2$, refer to the in-pile, monochromator-to-sample and sample-to-detector regions. η_M and η'_M are the horizontal and vertical mosaic spreads of the monochromator crystal while P_M is the reflectivity of that crystal for the most probable neutrons. θ_s is the scattering angle.

In Fig. 1 is shown a vector diagram in reciprocal space corresponding to the most probable scattering proces . The $\mathbf{k}$ axis of a Cartesian reference frame is chosen for convenience perpendicular to the plane of experiment defined by $\mathbf{k}_I$ and $\mathbf{k}_F$ The orientation of $\mathbf{i}$

axis given by the angle ϕ, is arbitrary. Making use of the measuring-angles convention, described in Table 1, $\mathbf{k}_I, \mathbf{k}_F, \mathbf{k}_i$ and $\mathbf{k}_f$ may be written as follows:

$$\begin{aligned}
\mathbf{k}_I &= k_I \cos\phi\mathbf{i} + k_I \sin\phi\mathbf{j} \\
\mathbf{k}_F &= k_I \cos(\phi+\theta_s)\mathbf{i} + k_I \sin(\phi+\theta_s)\mathbf{j} \\
\mathbf{k}_i &= k_i \cos(\phi+\gamma_1)\,\mathrm{ccs}\,\delta_1\mathbf{i} \\
&\quad + k_i \sin(\phi+\gamma_1)\cos\delta_1\mathbf{j} + k_i \sin\delta_1\mathbf{k} \\
\mathbf{k}_f &= k_f \cos(\phi+\theta_s+\gamma_2)\cos\delta_{2i} \\
&\quad + k_f \sin(\phi+\theta_s+\gamma_2)\cos\delta_2\mathbf{j} + k_f \sin\delta_2\mathbf{k}. \qquad (22)
\end{aligned}$$

The monochromator and analyser transmission functions are expressed in simple forms in terms of k_i, γ_1, γ_2, δ_1 and δ_2. Thus:

$$\begin{aligned}
T_M(\mathbf{k}_i, \mathbf{k}_I) &= T_{MH}(k_i, \gamma_1) T_{MV}(\delta_1) \\
T_A(\mathbf{k}_f, \mathbf{k}_F) &= T_{AH}(\gamma_2) T_{AV}(\delta_2)
\end{aligned}$$

where T_{MH} and T_{MV} are the horizontal and vertical transmission functions of the monochromator:

$$T_{MH}(k_i, \gamma_1) = P_M \exp\left\{-\left[\frac{1}{2\alpha_0^2}\left(\gamma_1 + 2\,\frac{k_i - k_I}{k_I}\,\mathrm{tg}\,\theta_M\right)^2 + \frac{1}{2\eta_M^2}\left(\gamma_1 + \frac{k_i - k_I}{k_I}\,\mathrm{tg}\,\theta_M\right)^2 + \frac{\gamma_1^2}{2\alpha_1^2}\right]\right\} \qquad (23)$$

$$T_{MV}(\delta_1) = \frac{\beta_0}{(\beta_0^2 + 4\eta_M'^2 \sin^2\theta_M)^{1/2}} \times \exp - \left\{\delta_1^2\left[\frac{1}{2\beta_0^2 + 8\eta_M'^2 \sin^2\theta_M} + \frac{1}{2\beta_1^2}\right]\right\}; \qquad (24)$$

T_{AH} and T_{AV} are the horizontal and vertical transmission functions of the analyser:

$$T_{AH}(\gamma_2) = \exp\left(-\frac{\gamma_2^2}{2\alpha_2^2}\right) \qquad (25)$$

$$T_{AV}(\delta_2) = \exp\left(-\frac{\delta_2^2}{2\beta_2^2}\right). \qquad (26)$$

For the actual values of the collimation angles and of the monochromator mosaic spread, the transmission functions (23)–(26) are measurably different from zero only when γ_1, γ_2, δ_1 and δ_2 do not exceed one or two degrees and $|k_i - k_I| \ll k_I$. On the other hand, for quasielastic cross sections, in the special experimental conditions discussed in the main text, the energy distribution in the scattered neutron beam takes essentially non-zero values only if $|k_f - k_I| \ll k_I$. Under these circumstances:

(*a*) All the integration limits in the expression obtained from equation (2), replacing the variables $\mathbf{k}_i$ and $\mathbf{k}_f$ by $u_1 = (k_i - k_I)\,\mathrm{tg}\,\theta_M/k_I$, $u_2 = k_f - k_I$, γ_1, γ_2, δ_1 and δ_2, may be extended to $(-\infty, +\infty)$ without introducing an appreciable error in the value of the integral.

(*b*) The slowly varying functions of k_i and k_f may be replaced by their values in k_I.

(*c*) The small-angle approximation may be used in equations (22) for γ and δ.

The next step is to replace the variables γ_1, γ_2, u_2 and δ_2 by $\mathbf{X} = \mathbf{Q} - \mathbf{Q}_0$ and $X_4 = (\hbar/2m)(k_i^2 - k_f^2)$. When the scattering angles are much larger than the collimations, γ_1, γ_2, u_2 and δ_2 are given by:

$$\begin{aligned}
\gamma_1 &= A_{10}u_1 + A_{11}X_1 + A_{12}X_2 + A_{14}X_4 \\
\gamma_2 &= A_{20}u_1 + A_{21}X_1 + A_{22}X_2 + A_{24}X_4 \\
u_2 &= A_{30}u_1 + A_{31}X_1 + A_{32}X_2 + A_{34}X_4
\end{aligned} \qquad (27)$$

and

$$\delta_2 = \delta_1 - X_3/k_I \qquad (28)$$

where:

$$\begin{aligned}
A_{10} &= \frac{\mathrm{tg}\,(\theta_s/2)}{\mathrm{tg}\,\theta_M} & A_{11} &= \frac{\cos(\phi+\theta_s)}{k_I \sin\theta_s} \\
A_{12} &= \frac{\sin(\phi+\theta_s)}{k_I \sin\theta_s} & A_{14} &= \frac{-(m/\hbar)}{k_I^2 \sin\theta_s} \\
A_{20} &= -A_{10} & A_{21} &= \frac{\cos\phi}{k_I \sin\theta_s} \\
A_{22} &= \frac{\sin\phi}{k_I \sin\theta_s} & A_{24} &= \frac{-(m/\hbar)\cos\theta_s}{k_I^2 \sin\theta_s}
\end{aligned} \qquad (29)$$

$$A_{30} = k_I/\mathrm{tg}\,\theta_M \qquad A_{31} = A_{32} = 0 \qquad A_{34} = -m/(\hbar k_I).$$

When care has been taken to include the Jacobians of the variable transformations, after integration over u_1 and δ_1, there results the expression from equation (4) given in the main text, defining the resolution function as:

$$R(\mathbf{Q}_0, \mathbf{X}, X_4) = R_0(\mathbf{Q}_0) \exp\left(-\tfrac{1}{2}\sum_{i,j=1}^{4} M_{ij}X_iX_j\right) \qquad (30)$$

where:

$$R_0(\mathbf{Q}_0) = R_{0H}(\mathbf{Q}_0) R_{0V} \qquad (31)$$

and

$$M_{ij} = M_{ji}. \qquad (32)$$

For the description of R_{0H}, R_{0V} and M_{ij} some new definitions are introduced:

$$m_1 = \frac{1}{2\alpha_0^2}; \quad m_2 = \frac{1}{2\eta_M^2}; \quad m_3 = \frac{1}{2\alpha_1^2}; \quad a_1 = \frac{1}{2\alpha_2^2} \qquad (33)$$

$$M = m_1m_2 + 4m_1m_3 + m_2m_3 \qquad (34)$$

Table 1. *Measuring-angles convention*

Angle	Range	Origin	Positive sense
γ	$(-\pi, +\pi)$	The most probable **k**.	Trigonometrical
$\theta_s, 2\theta_M$	$(-\pi, +\pi)$	The most probable **k** incident.	Trigonometrical
ϕ	$(-\pi, +\pi)$	**i** axis.	Trigonometrical
δ	$(-\pi/2, +\pi/2)$	Projection of **k** on horizontal plane.	k_z positive.

$$S_1=(A_{10}+2)^2m_1+(A_{10}+1)^2m_2+A_{10}^2(m_3+a_1) \quad (35)$$

$$T_i(n)=A_{10}(A_{1i}+A_{2i})+(3-n)A_{2i} \quad (36)$$

$$v_1=\frac{1}{2\beta_0^2}\,;\quad v_2=\frac{1}{2\beta_0^2+8\eta_M'^2\sin^2\theta_M}\,;$$

$$v_3=\frac{1}{2\beta_1^2}\,;\quad V=\frac{1}{2\beta_2^2}\,. \quad (37)$$

Then:

$$R_{0H}=\frac{P_M}{|\sin\theta_s\,\mathrm{tg}\,\theta_M|}\left(\frac{\pi}{S_1}\right)^{1/2} \quad (38)$$

$$R_{0V}=\left[\frac{\pi v_2}{v_1(v_2+v_3+V)}\right]^{1/2}. \quad (39)$$

For $i,j=1,2,4$:

$$M_{ij}=\frac{2}{S_1}\left[MA_{1i}A_{1j}+a_1\sum_{n=1}^{3}T_i(n)T_j(n)m_n\right] \quad (40)$$

$$M_{3i}=0 \quad (41)$$

while:

$$M_{33}=\frac{2}{k_I^2}\cdot\frac{V(v_2+v_3)}{v_2+v_3+V}\,. \quad (42)$$

Derivation of the (Q,ω) resolution function

As in the general case, the deviations from the nominal values are used:

$$X=Q-Q_0$$
$$X_4=\omega\,. \quad (43)$$

When the **i** axis of the reference frame (see Fig. 1) is directed along $\mathbf{Q}_0$:

$$X=\frac{Q^2-Q_0^2}{Q+Q_0}\simeq X_1+\frac{X_1^2+X_2^2+X_3^2}{2Q_0}\simeq X_1\,. \quad (44)$$

The procedure for the resolution function calculation is similar to the one in the previous section. Thus X_1 and X_4 are introduced in the expression of the counting rate to replace two of the six variables $(u_1,\gamma_1,\delta_1,u_2,\gamma_2,\delta_2)$, say γ_1 and u_2.

From equations (27) and (29) there result:

$$\gamma_1=\gamma_2+B_{10}u_1+B_{11}X_1+B_{14}X_4$$
$$u_2=B_{30}u_1+B_{31}X_1+B_{34}X_4 \quad (45)$$

where:

$$B_{10}=2A_{10}$$

$$B_{11}=A_{11}-A_{21}=-\frac{\mathrm{sign}\,\theta_s}{k_I\cos(\theta_s/2)} \quad (46)$$

$$B_{14}=A_{14}-A_{24}=-\frac{(m/\hbar)}{k_I^2}\,\mathrm{tg}(\theta_s/2)$$

$$B_{3i}=A_{3i}\,.$$

The integration over the remaining variables gives the equation (6) defining the (Q,ω) resolution function as:

$$\mathcal{R}(Q_0,X_1,X_4)=\mathcal{R}_0(Q_0)\exp\left[-\tfrac{1}{2}(\mathcal{M}_{11}X_1^2+2\mathcal{M}_{14}X_1X_4+\mathcal{M}_{44}X_4^2)\right] \quad (47)$$

where:

$$\mathcal{R}_0(Q_0)=\frac{\pi P_M}{4|\mathrm{tg}\,\theta_M\cos(\theta_s/2)|}\cdot\frac{1}{(S_2)^{1/2}}\times\left[\frac{v_2}{v_1V(v_2+v_3)}\right]^{1/2} \quad (48)$$

and:

$$\mathcal{M}_{ij}=\frac{2Ma_1B_{1i}B_{1j}}{S_2}\,. \quad (49)$$

S_2 is given by:

$$S_2=M+a_1[(B_{10}+2)^2m_1+(B_{10}+1)^2m_2+B_{10}^2m_3]. \quad (50)$$

Bragg peaks of a perfect crystal

When the **i** axis of the reference frame is in the opposite direction to a certain reciprocal vector of the sample, *i.e.* $\tau=-\tau_1$, according to equation (13) the corresponding Bragg peak is described by:

$$I(\mathbf{Q}_0)=I(\theta_B)\exp\left[-\tfrac{1}{2}M_{11}(Q_{01}-2\pi\tau)^2+2M_{12}(Q_{01}-2\pi\tau)Q_{02}+M_{22}Q_{02}^2\right] \quad (51)$$

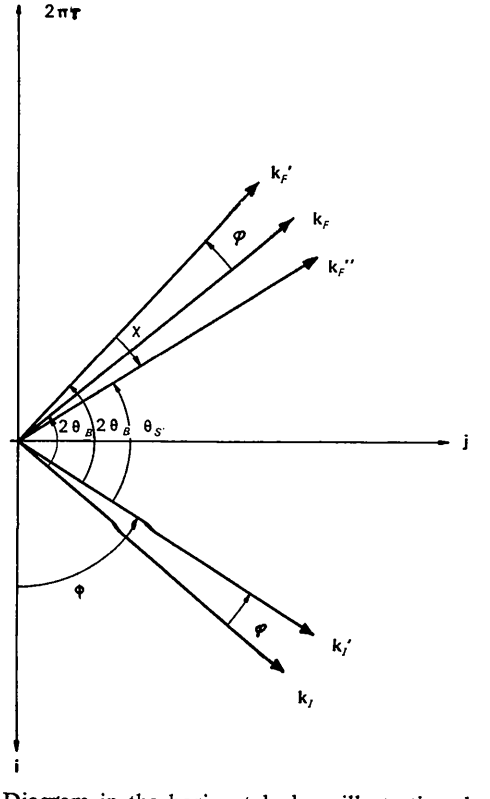

Fig. 2. Diagram in the horizontal plane illustrating the relationship between mis-setting angles and the most probable wave vectors.

where $I(\theta_B)$ represents the peak intensity, occuring when

$$Q_{02}=k_I[\sin\phi-\sin(\phi+\theta_s)]=0 \tag{52}$$

and

$$Q_{01}=k_I[\cos\phi-\cos(\phi+\theta_s)]=2\pi\tau=2k_I|\sin\theta_B|. \tag{53}$$

The condition (52) leads to:

$$\phi=(\pi/2)\ \text{sign}\ \theta_s-\theta_s/2 \tag{54}$$

while (53) demands:

$$\theta_s=2\theta_B. \tag{55}$$

The shape of the peak is dependent on scanning procedure. In our particular reference frame $\mathbf{Q}_0$ may be changed by rotating $\mathbf{k}_I$ and $\mathbf{k}_F$ about a vertical axis. The rotation of the sample through an angle $-\varphi$ from the optimum position (see Fig. 2) is equivalent to the rotation of both $\mathbf{k}_I$ and $\mathbf{k}_F$, through an angle φ, to position $\mathbf{k}_I'$ and $\mathbf{k}_F'$, the scattering angle remaining equal to $2\theta_B$. The detector rotation by an angle χ represents a rotation of $\mathbf{k}_F'$ through the same angle, to $\mathbf{k}_F''$. In this configuration:

$$\phi=(\pi/2)\ \text{sign}\ \theta_B-\theta_B+\varphi \tag{56a}$$

$$\theta_s=2\theta_B+\chi \tag{56b}$$

and consequently:

$$Q_{01}-2\pi\tau=k_I\chi\cos\theta_B \tag{57a}$$

$$Q_{02}=k_I(\chi+2\varphi)\sin\theta_B. \tag{57b}$$

At a rotation of the reference frame (*i.e.* of the sample) through a small angle ψ (comparable with the vertical collimation angles) about the **j** axis, the components of the scattering vector are changed in the following way:

$$\begin{aligned}&Q_{01}'=Q_{01}\cos\psi\simeq Q_{01}\\&Q_{02}'=Q_{02}\\&Q_{03}'=Q_{01}\sin\psi\simeq\psi(2\pi\tau+k_I\chi\cos\theta_B)\simeq 2k_I\psi\sin\theta_B.\end{aligned} \tag{58}$$

As it may be seen in equations (58) the horizontal component of the scattering vector is not changed when ψ is a small quantity; the greater ψ values are not important owing to the vertical collimation. Consequently, all the results obtained so far under the oversimplifying condition $Q_{03}=0$ remain valid and the counting rate for a general configuration defined by mis-setting angles φ, χ and ψ is given by:

$$I(\theta_B,\mathbf{q})=I(\theta_B)\exp[-\tfrac{1}{2}(M_{11}q_1^2+2M_{12}q_1q_2+M_{22}q_2^2+M_{33}q_3^2)] \tag{59}$$

where

$$q_i=Q_{0i}+2\pi\tau_i.$$

According to equations (57) and (58):

$$q_1=k_I\chi\cos\theta_B \tag{60a}$$

$$q_2=k_I(\chi+2\varphi)\sin\theta_B \tag{60b}$$

$$q_3=2k_I\psi\sin\theta_B. \tag{60c}$$

The elements of the resolution function from equation (59) are given by equations (38)–(42) in which, in agreement with equations (54) and (55), $\phi=(\pi/2)\ \text{sign}\ \theta_B-\theta_B$ and $\theta_s=2\theta_B$.

Hence:

$A_{10}=-A_{20}=\text{tg}\,\theta_B/\text{tg}\,\theta_M=a=$dispersion parameter (Caglioti, Paoletti & Ricci, 1958)

$$A_{11}=-A_{21}=-\frac{\text{sign}\ \theta_B}{2k_I\cos\theta_B} \tag{61}$$

$$A_{12}=A_{22}=\frac{\text{sign}\ \theta_B}{2k_I\sin\theta_B}.$$

Then:

$$S_1=(a+2)^2m_1+(a+1)^2m_2+a^2(m_3+a_1) \tag{62}$$

and:

$$M_{11}=\frac{l_{11}}{2S_1k_I^2\cos^2\theta_B}\qquad M_{22}=\frac{l_{22}}{2S_1k_I^2\sin^2\theta_B}$$

$$M_{12}=\frac{l_{12}}{2S_1k_I^2\sin\theta_B\cos\theta_B}\qquad M_{33}=\frac{l_{33}}{2k_I^2\sin^2\theta_B} \tag{63}$$

where:

$$\begin{aligned}l_{11}&=M+(4m_1+m_2)a_1\\l_{12}&=-M+[4(a+1)m_1+(2a+1)m_2]a_1\\l_{22}&=M+[4(a+1)^2m_1+(2a+1)^2m_2+4a^2m_3]a_1\\l_{33}&=4V(v_2+v_3)\sin^2\theta_B/(v_2+v_3+V).\end{aligned} \tag{64}$$

The maximum intensity is obtained when $\mathbf{q}=0$, *i.e.* $\chi=\varphi=\psi=0$; it may be written as:

$$I(\theta_B)=\frac{C_s}{(\pi S_1)^{1/2}}\cdot\left[\frac{v_2}{v_1(v_2+v_3+V)}\right]^{1/2} \tag{65}$$

where C_s is a proportionality factor:

$$C_s=(2\pi/\pi)^3\Phi(\mathbf{k}_I)\varepsilon(k_I)\frac{N|F|^2}{V_c|\sin 2\theta_B|}\frac{P_M}{|\text{tg}\,\theta_M|}. \tag{66}$$

Introducing the coordinates defined in equations (15) there results:

$$q_{\xi\zeta}=k_I[\chi^2+4(\chi\varphi+\varphi^2+\psi^2)\sin^2\theta_B]^{1/2} \tag{67a}$$

$$\xi=\text{arctg}\left(\frac{\chi+2\varphi}{\chi}\,\text{tg}\,\theta_B\right) \tag{67b}$$

$$\zeta=\text{arctg}\left(\frac{2\psi\,\text{tg}\,\theta_B}{[\chi^2+(\chi+2\varphi)^2\,\text{tg}^2\,\theta_B]^{1/2}}\right). \tag{67c}$$

Equations (19) and (20) from the main text together with the above formulae make possible the calculation of the width and integrated intensity for any linear scan. Some conventional scans will be discussed below.

Crystal (φ) scan

In the (φ) scan, the sample crystal is rotated about a vertical axis keeping the detector fixed in the Bragg

position. In this situation $\chi=\psi=0$ and according to equations (67) $\xi=\pi/2$ and $\zeta=0$. Then $q_1=q_3=0$, *i.e.* the equi-intensity ellipsoids are scanned along the **j** axis. Therefore:

$$I_\varphi=I(\theta_B)\left(\frac{2\pi}{M_{22}}\right)^{1/2} \tag{68a}$$

$$L_\varphi=\left(\frac{2\ln 2}{M_{22}}\right)^{1/2}. \tag{68b}$$

In equations (68) I_φ and L_φ are expressed in units of Q. However, usually the Bragg peaks are plotted in terms of angular units. Equations (68) may be re-written on a φ scale by dividing them by a scale factor equal to $2k_I|\sin\theta_B|$, as obtained from equation (67*a*). Hence, on a φ scale, the peak integrated intensity and half width are given by:

$$\mathscr{I}_\varphi=\frac{C_s}{(l_{22})^{1/2}}\left[\frac{v_2}{v_1(v_2+v_3+V)}\right]^{1/2} \tag{69a}$$

$$\mathscr{L}_\varphi=\left(\frac{\ln 2S_1}{l_{22}}\right)^{1/2}. \tag{69b}$$

Crystal–detector $(\varphi,-2\varphi)$ *scan*

In this scan $\chi=-2\varphi$ and $\psi=0$. Then $\xi=\zeta=0$ and $q_1=q_3=0$, *i.e.* the scanning is performed along the **i** axis. Hence

$$I_{\varphi,-2\varphi}=I(\theta_B)\left(\frac{2\pi}{M_{11}}\right)^{1/2} \tag{70a}$$

$$L_{\varphi,-2\varphi}=\left(\frac{2\ln 2}{M_{11}}\right)^{1/2} \tag{70b}$$

while on the φ-scale:

$$\mathscr{I}_{\varphi,-2\varphi}=\frac{C_s}{(l_{11})^{1/2}}\left[\frac{v_2}{v_1(v_2+v_3+V)}\right]^{1/2} \tag{71a}$$

$$\mathscr{L}_{\varphi,-2\varphi}=\left(\frac{\ln 2S_1}{l_{11}}\right)^{1/2}. \tag{71b}$$

The scale factor is now $2k_I|\cos\theta_B|$.

Detector (χ) *scan*

When the crystal is kept fixed in the Bragg position and the detector is rotated ($\varphi=\psi=0$), $\xi=\theta_B$ and $\zeta=0$. Then:

$$q_1=k_I\chi\cos\theta_B$$
$$q_2=k_I\chi\sin\theta_B$$
$$q_3=0$$

and consequently:

$$I_\chi=I(\theta_B)\times\left[\frac{2\pi}{M_{11}\cos^2\theta_B+2M_{12}\cos\theta_B\sin\theta_B+M_{22}\sin^2\theta_B}\right]^{1/2} \tag{72a}$$

$$L_\chi=\left[\frac{2\ln 2}{M_{11}\cos^2\theta_B+2M_{12}\cos\theta_B\sin\theta_B+M_{22}\sin^2\theta_B}\right]^{1/2}. \tag{72b}$$

On the χ scale (scaling factor k_I):

$$\mathscr{I}_\chi=\frac{C_s}{[(S_1-a^2a_1)a_1]^{1/2}}\left[\frac{v_2}{v_1(v_2+v_3+V)}\right]^{1/2} \tag{73a}$$

$$\mathscr{L}_\chi=\left[\frac{\ln 2S_1}{(S_1-a^2a_1)a_1}\right]^{1/2}. \tag{73b}$$

Vertical (ψ) *scan*

If the crystal is rotated from the Bragg position about the **j** axis ($\varphi=\chi=0$), $\zeta=\pi/2$, *i.e.* the scanning is performed along the **k** axis. The integrated intensity and half width of the peak are in this case given by:

$$I_\psi=I(\theta_B)\left(\frac{2\pi}{M_{33}}\right)^{1/2} \tag{74a}$$

$$L_\psi=\left(\frac{2\ln 2}{M_{33}}\right)^{1/2}. \tag{74b}$$

On the ψ_I scale (scaling factor $2k\,|\sin\theta_B|$):

$$\mathscr{I}_\psi=\frac{C_s}{2|\sin\theta_B|\,(S_1)^{1/2}}\left[\frac{v_2}{v_1V(v_2+v_3)}\right]^{1/2} \tag{75a}$$

$$\mathscr{L}_\psi=\left(\frac{\ln 2}{l_{33}}\right)^{1/2}. \tag{75b}$$

Bragg peaks of a mosaic imperfect crystal

If a certain reciprocal vector of the most probable mosaic blocks is in the opposite direction to the **i** axis (*i.e.* $\tau=-\tau\mathbf{i}$), the corresponding reciprocal vector attached to a mosaic block described by the horizontal and vertical mosaic angles φ_1 and ψ_1, respectively, is given by:

$$\tau'\simeq-\tau\mathbf{i}+\tau\varphi_1\mathbf{j}+\tau\psi_1\mathbf{k}\,.$$

Then:

$$\frac{\mathrm{d}\sigma_m}{\mathrm{d}\Omega}=\int\frac{\mathrm{d}\sigma}{\mathrm{d}\Omega}[\tau'(\varphi_1,\psi_1)]\mathscr{P}(\varphi_1)\mathscr{P}(\psi_1)\mathrm{d}\varphi_1\mathrm{d}\psi_1$$

where $\mathscr{P}(\varphi_1)$ and $\mathscr{P}(\psi_1)$ are the distribution functions of the mosaic angles. When they are Gaussians with half widths $\mathscr{L}_{SH}=(2\ln 2)^{1/2}\eta_S$ and $\mathscr{L}_{SV}=(2\ln 2)^{1/2}\eta_S'$ respectively, the scattering cross section becomes:

$$\frac{\mathrm{d}\sigma_m}{\mathrm{d}\Omega}=\frac{|F|^2}{V_c\tau^2\eta_S\eta_S'}\exp\left[-(Q_2^2/\eta_S^2+Q_3^2/\eta_S'^2)/(8\pi^2\tau^2)\right]\delta(Q_1-2\pi\tau)\,.$$

Introducing this into equation (9) leads to expression (21) for the counting rate, where:

$$I'(\theta_B)=\frac{I(\theta_B)}{\left[\left((2\eta_S^2\frac{l_{22}}{S_1}+1\right)(2\eta_S'^2l_{33}+1)\right]^{1/2}}, \tag{76}$$

while the M'_{ij} are given by the same formulae as M_{ij} [equations (63)] in which the l_{ij} are replaced by l'_{ij}:

$$l'_{11}=(8\eta_S^2 a_1 M+l_{11})/\left(2\eta_S^2\frac{l_{22}}{S_1}+1\right)$$
$$l'_{12}=l_{12}/\left(2\eta_S^2\frac{l_{22}}{S_1}+1\right)$$
$$l'_{22}=l_{22}/\left(2\eta_S^2\frac{l_{22}}{S_1}+1\right)$$
$$l'_{33}=l_{33}/(2\eta_S'^2 l_{33}+1)\,. \qquad (77)$$

As indicated in the main text the derivation of the results from Table 2 is now straightforward. In the limiting case, $\eta_S=\eta'_S=0$, these results are reduced to those corresponding to a perfect crystal.

A particular case, important in practice, is worth remembering: in a parallel setting of two identical crystals (which may have different mosaic spreads), with relaxed horizontal collimation between them, $a=-1$, $m_3=0$, and consequently:

$$\mathscr{L}'^2_\varphi=2\ln 2(\eta_M^2+\eta_S^2) \qquad (78a)$$
$$\mathscr{L}'^2_x=\mathscr{L}^2_x=2\ln 2(\alpha_0^2+\alpha_2^2). \qquad (78b)$$

Diffraction pattern of a polycrystal

Introducing in equation (10) the coherent elastic-scattering cross section of a polycrystal

$$\frac{d\sigma_p}{d\Omega}=\frac{1}{2V_c}\sum_\tau\frac{n_\tau}{\tau^2}|F(Q)|^2\delta(Q-2\pi\tau)\,,$$

there results the following equation for the diffraction pattern:

$$I(Q_0)=\Phi(k_I)\varepsilon(k_I)\frac{N}{2V_c}\sum_\tau\frac{n_\tau}{\tau^2}|F(2\pi\tau)|^2\mathscr{R}_0(2\pi\tau)\times\exp\left[-\tfrac{1}{2}\mathscr{M}_{11}(Q_0-2\pi\tau)^2\right],$$

were n_τ is the multiplicity factor.

For a certain τ, the maximum intensity is obtained when $Q_0=2\pi\tau$, *i.e.*

$$\theta_s=2\theta_B. \qquad (80)$$

In a general position defined by the detector mis-setting angle χ, $\chi=\theta_s-2\theta_B$, the magnitude of the scattering vector is given by:

$$Q_0=2\pi\tau+k_I\chi\cos\theta_B. \qquad (81)$$

According to equations (48), (49) and (80)

$$\mathscr{R}_0(2\pi\tau)=\frac{\pi P_M}{4|\mathrm{tg}\,\theta_M\cos\theta_B|(l_{22})^{1/2}}\left[\frac{v_2}{v_1V(v_2+v_3)}\right]^{1/2} \qquad (82a)$$

$$\mathscr{M}_{11}(2\pi\tau)=\frac{2Ma_1}{k_I^2\cos^2\theta_B l_{22}}\,. \qquad (82b)$$

Then the counting rate becomes:

$$I(Q_0)=I(\theta_B)\exp\left(-\frac{Ma_1}{l_{22}}\chi^2\right), \qquad (83)$$

where $I(\theta_B)$ represents the maximum intensity:

$$I(\theta_B)=\frac{C_p}{(\pi l_{22})^{1/2}}\left[\frac{v_2}{v_1V(v_2+v_3)}\right]^{1/2}. \qquad (84)$$

C_p is a proportionality factor:

$$C_p=\frac{n_\tau C_s}{8|\sin\theta_B|}\,. \qquad (85)$$

Consequently, on the χ scale, the integrated intensities and half widths of Bragg peaks of a polycrystal are given by:

$$\mathscr{L}_\chi=\left(\frac{\ln 2 l_{22}}{M}\right)^{1/2} \qquad (86a)$$

$$\mathscr{I}_\chi=\frac{C_p}{(Ma_1)^{1/2}}\left[\frac{v_2}{v_1V(v_2+v_3)}\right]^{1/2}. \qquad (86b)$$

When the Q units are used (scale factor $k_I|\cos\theta_B|$):

$$L_\chi=k_I|\cos\theta_B|\mathscr{L}_\chi \qquad (87a)$$
$$I_\chi=k_I|\cos\theta_B|\mathscr{I}_\chi\,. \qquad (87b)$$

Table 2. *The half widths and integrated intensities of Bragg peaks of a mosaic crystal*

Scan	Definition	Scale	Half width	Integrated intensity
(φ)	$\chi=0$	φ	$\mathscr{L}'_\varphi=[\ln 2(S_1/l_{22}+2\eta_S^2)]^{1/2}$	$\mathscr{I}'_\varphi=\frac{C_s}{(l_{22})^{1/2}}\left[\frac{v_2}{v_1(v_2+v_3+V)(2\eta_S'^2 l_{33}+1)}\right]^{1/2}$
	$\psi=0$		$=(\mathscr{L}^2_\varphi+\mathscr{L}^2_{SH})^{1/2}$	
$(\varphi,-2\varphi)$	$\chi=-2\varphi$			
	$\psi=0$	φ	$\mathscr{L}'_{\varphi,-2\varphi}=\left[\ln 2\,\frac{S_1+2\eta_S^2 l_{22}}{l_{11}+8\eta_S^2 a_1 M}\right]^{1/2}$	$\mathscr{I}'_{\varphi,-2\varphi}=\frac{C_s}{(l_{11}+8\eta_S^2 a_1 M)^{1/2}}\left[\frac{v_2}{v_1(v_2+v_3+V)(2\eta_S'^2 l_{33}+1)}\right]^{1/2}$
(χ)	$\varphi=0$	χ	$\mathscr{L}'_\psi=\left[\ln 2\,\frac{S_1+2\eta_S^2 l_{22}}{a_1(S_1-a^2a_1)+2\eta_S^2 a_1 M}\right]^{1/2}$	$\mathscr{I}'_x=\frac{C_s}{[a_1(S_1-a^2a_1)+2\eta_S^2 a_1 M]^{1/2}}\left[\frac{v_2}{v_1(v_2+v_3+V)(2\eta_S'^2 l_{33}+1)}\right]^{1/2}$
	$\psi=0$			
(ψ)	$\varphi=0$	ψ	$\mathscr{L}'_\psi=[\ln 2(1/l_{33}+2\eta_S'^2)]^{1/2}$	$\mathscr{I}'_\psi=\frac{C_s}{[l_{33}(2\eta_S^2 l_{22}/S_1+1)]^{1/2}}\left[\frac{v_2}{v_1(v_2+v_3+V)}\right]^{1/2}$
	$\chi=0$		$=(\mathscr{L}^2_\psi+\mathscr{L}^2_{SV})^{1/2}$	

The incoherent background

Assuming the Debye–Waller factor is a slowly varying function of Q, the counting rate due to the incoherent scattering is obtained from equations (10), (48) and (49):

$$I_{\text{inc}} = \frac{C_{\text{inc}}}{(Ma_1)^{1/2}} \left[\frac{v_2}{v_1 V(v_2+v_3)}\right]^{1/2} \tag{88}$$

where:

$$C_{\text{inc}} = \pi^2 \mathcal{V} \pi \Phi(\mathbf{k}_I)\varepsilon(k_I) N k_I^3 \frac{\mathrm{d}\sigma_{\text{inc}}}{\mathrm{d}\Omega} \frac{P_M}{|\mathrm{tg}\,\theta_M|}. \tag{89}$$

References

CAGLIOTI, G., PAOLETTI, A. & RICCI, F. P. (1958). *Nucl. Instrum. Meth.* **3**, 223–228.

CAGLIOTI, G., PAOLETTI, A. & RICCI, F. P. (1960). *Nucl. Instrum. Meth.* **9**, 195–198.

CAGLIOTTI, G. & RICCI, F. P. (1962). *Nucl. Instrum. Meth.* **15**, 155–163.

CASSELS, J. M. (1950). *Progr. Nucl. Phys.* **1**, 185–215.

COOPER, M. J. (1968). *Acta Cryst.* A**24**, 624–627.

COOPER, M. J. & NATHANS, R. (1967). *Acta Cryst.* **23**, 357–367.

COOPER, M. J. & NATHANS, R. (1968*a*). *Acta Cryst.* A**24**, 481–484.

COOPER, M. J. & NATHANS, R. (1968*b*). *Acta Cryst.* A**24**, 619–624.

GRABCEV, B. (1973*a*). Report IFA-FN-43, Institute for Atomic Physics, Bucharest.

GRABCEV, B. (1973*b*). *Nucl. Instrum. Meth.* **106**, 349–355.

SAILOR, V. L., FOOTE, H. L. JR, LANDON, H. H. & WOOD, R. E. (1956). *Rev. Sci. Instrum.* **27**, 26–34.

TEUTSCH, H. (1971). *Stud. Cerc. Fiz.* **23**, 517–553.

TUCCIARONE, A., LAU, H. Y., CORLISS, L. M., DELAPALME, A. & HASTINGS, J. M. (1971). *Phys. Rev.* B**4**, 3206–3245.

WILLIS, B. T. M. (1960). *Acta Cryst.* **13**, 763–766.

Acta Cryst. (1974). A**30**, 216

Interpretation of Short-Range-Order Scattering of Electrons; Application to Ordering of Defects in Vanadium Monoxide

BY B. ANDERSSON, J. GJØNNES AND J. TAFTØ

Department of Physics, University of Oslo, Oslo, Norway

(*Received* 16 *July* 1973; *accepted* 19 *September* 1973)

Diffuse scattering of electrons from local order of defects in vanadium monoxide of composition $VO_{1.23}$ has been studied above the ordering temperature. Intensity expressions for short-range-order scattering involving defects of more than one kind are derived, both for the kinematical case and with Bragg scattering effects included. The interpretation is based upon comparison between experimental and calculated distributions in intensity space and vector space, mainly in projections where Bragg scattering effects are small or moderate. The scattering can be interpreted in terms of defect clusters consisting of one metal interstitial surrounded by four metal vacancies, as in the ordered structure $V_{52}O_{64}$. The local arrangement of clusters is different from that found in the ordered phase, however.

1. Introduction

The ease with which patterns of diffuse scattering from single crystals can be obtained in electron diffraction has made it a useful tool for the study of local order of defects. However, emphasis in applications has almost exclusively been on the qualitative side. Quantitative interpretation of diffuse scattering in terms of order parameters, as was developed in the X-ray case some 20 years ago, has been tried only to a very limited extent. The main reasons for this are associated with the strong interaction between the incident electron and the crystal. This may call for more complicated intensity expressions than those given by kinematical theory, especially when strong Bragg reflexions are excited, and will also render the extraction of short-range-order scattering from other types of diffuse scattering more difficult.

General expressions for diffuse scattering of electrons including dynamical interactions through Bragg reflexions have previously been developed (Gjønnes, 1965, 1966; Gjønnes & Höier, 1971). It was found that substitutional short-range order in binary alloys represents a relatively simple case (Fisher, 1965), the Bragg scattering effects leading mainly to a redistribution of diffuse scattering between different Brillouin zones. When more than one lattice site is involved in the ordering, the situation becomes more complicated, but also more interesting, since the Bragg scattering effects on the diffuse scattering may then introduce features which carry information which is not contained in purely kinematical experiments.

Our reasons for starting a study on the vanadium–oxygen system stemmed, to some extent, from such considerations. The defect rocksalt-type oxides of transition metals (TiO, FeO, VO, *etc.*) contain many de-